

Baseband Macromodeling of Linear Photonic Circuits for Time-Domain Simulations

Yinghao Ye , *Student Member, IEEE*, Domenico Spina , *Member, IEEE*, Wim Bogaerts , *Senior Member, IEEE*, and Tom Dhaene , *Senior Member, IEEE*

Abstract—In this paper, we propose a novel approach to build real-valued baseband models of linear, time-invariant, passive photonic devices, circuits, and systems, which allows modeling of photonic wavelength filter circuits with their full dispersion effects in an accurate way. The proposed technique starts from the scattering parameters of the photonic systems under study and leverages on the modeling power of the vector-fitting algorithm, thereby leading to both complex- and real-valued baseband state-space models. The modeling procedure is robust and applicable to general linear passive photonic devices and circuits, and the physical properties of the resulting models for the time-domain simulation, such as stability and passivity, can be properly guaranteed. The built models are systems of first-order ordinary differential equations (ODEs), which can be efficiently simulated in a variety of ODE solvers at baseband frequencies rather than in the optical frequency range. We demonstrate the applicability and accuracy of the proposed method on two examples of photonic filter circuits.

Index Terms—Baseband modeling, photonic integrated circuits, state-space representation, system identification, time-domain analysis.

I. INTRODUCTION

OVER the last decade, *photonic integrated circuits* (PIC), and especially *silicon photonics*, gained a lot of popularity due to their compatibility with the manufacturing processes used in the CMOS industry. Given the rapid development of PIC in terms of complexity and integration scale, *photonic design automation* (PDA) tools for photonic circuit simulations, or photonic-electronic co-simulation [1]–[4], become of paramount importance.

In this framework, it is fundamental to build compact models which can accurately and efficiently mimic the behavior of photonic devices and circuits, for both frequency-domain and time-domain simulations. In this paper, we focus on the modeling of linear passive devices and systems whose functions roughly

fall into two categories: distributing/transporting light (e.g. waveguides), and optical wavelength filtering for applications such as spectroscopy, *wavelength division multiplexing* (WDM) or *microwave photonics* (MWP) applications. Especially in the last two applications, an efficient modeling approach of the filters, which is able to take into account imperfections such as higher-order dispersion, wavelength-dependent loss, and imperfections in coupling coefficients, is urgently needed.

A common approach is to compute analytic models, which rely on the knowledge of the working principles of the device under study. Such models are useful in the design phase, because the geometrical or optical parameters (such as length, coupling coefficient, effective index, etc.) are directly related to the performance measures of the device considered. However, in practice, analytic models can be derived only for simple photonic systems and there is a limit in their accuracy when describing complex non-ideal characteristics of the system under study (i.e. backscattering and undesired dispersion effects). Furthermore, most of these models are generally described as frequency- (wavelength) domain models, whereas time-domain models are needed when time-domain simulations are required to evaluate the performance of the PIC, such as bit error rate or eye diagrams [1], [3].

In practice, for passive devices and circuits, their scattering parameters data are more accessible (e.g. via electromagnetic simulations or measurements) than accurate analytic models. Hence, it is convenient to conduct time-domain simulations starting from the scattering parameters.

A typical example is given by the *finite impulse response* (FIR) modeling technique [5], which is based on the scattering parameters representation and is adopted in the dedicated photonic simulator Lumerical INTERCONNECT [6]. The accuracy provided by FIR filters substantially depends on the design methodology employed and it inherently degrades near the edges of the simulated signal bands [5]. Recently, we proposed a novel baseband state-space modeling approach [7], which employs the robust *vector fitting* (VF) algorithm [8]–[10] to build macromodels which operate at the baseband with complex signals. The term *macromodel* is adopted here to indicate that the modeling procedure describes the system behavior as seen from its inputs/outputs (I/O) ports. The proposed modeling approach starts from the scattering parameters of the system under study and allows one to build a model in state-space form representing general linear and passive multiports photonic systems. Such model operating at optical frequency range can

Manuscript received October 2, 2018; revised December 23, 2018; accepted January 14, 2019. Date of publication January 16, 2019; date of current version February 22, 2019. This work was supported in part by Research Foundation-Flanders (FWO-Vlaanderen) under Grant G013815N. (*Corresponding author: Yinghao Ye.*)

Y. Ye, D. Spina, and T. Dhaene are with the Internet Technology and Data Science Lab, Department of Information Technology, Ghent University-imec, 9052 Ghent, Belgium (e-mail: yinghao.ye@ugent.be; domenico.spina@ugent.be; tom.dhaene@ugent.be).

W. Bogaerts is with the Photonics Research Group, Department of Information Technology, Ghent University-imec, 9052 Ghent, Belgium (e-mail: wim.bogaerts@ugent.be).

Color versions of one or more of the figures in this paper are available online at <http://ieeexplore.ieee.org>.

Digital Object Identifier 10.1109/JLT.2019.2893545

then be converted into an equivalent complex-valued baseband state-space representation, which is inherently a system of first-order *ordinary differential equations* (ODE) and it can be efficiently simulated in ODE solvers [7], such as the Matlab routine *lsim*. It is important to remark that the method proposed in [7] requires to compute a specific type of complex-valued state-space representation via the VF algorithm and the corresponding system of ODE must be solved in simulators able to handle complex-valued signals and matrices.

In this contribution, first the modeling framework proposed in [7] is generalized to a wider range of state-space representations of photonic systems, which can be computed by means of the VF algorithm or other system identification techniques, such as *model order reduction* (MOR) approaches. Next, the obtained complex-valued baseband model is converted into a new, real-valued state-space model. Given that the new model retains the computational efficiency of the corresponding complex-valued baseband representation, we call it the *real-valued baseband model* in the rest of the contribution. However, differently from its complex-valued counterpart, which is a pure mathematical representation of the photonic system under study defined only to speed-up time-domain simulations, the real-valued baseband model retains the properties of a physical system. In particular, since stability and passivity are essential for time-domain simulations [11], it is rigorously proven that the new real-valued baseband model is stable and passive if the original state-space model computed at optical frequencies is stable and passive as well.

The paper is organized as follows. Section II gives an overview of the baseband modeling technique proposed in [7], and then Section III presents the novel complex-valued baseband modeling framework. The proposed real-valued baseband model is described in Section IV and its properties are rigorously discussed. Section V presents two suitable numerical examples validating the accuracy and efficiency of the proposed methods, and conclusions are drawn in Section VI.

II. BASEBAND MODELING FRAMEWORK OF LINEAR PHOTONIC SYSTEMS

The frequency range of interest for photonic systems is typically around [187; 200] THz, corresponding to a wavelength of [1.5; 1.6] μm , commonly used for telecommunication applications. Such a wide range at high frequencies has a direct impact on the modeling and simulation processes, which can become very time and/or memory consuming.

The baseband modeling and simulation approach proposed in [7] splits the optical carrier frequency from both the port signals and systems, and allows one to operate at baseband: the resulting models can be simulated with high accuracy and efficiency. In particular, the excitation signals of photonic systems are defined in [7] as amplitude and/or phase electronic modulated signals over an optical carrier with frequency f_c , as

$$a(t) = A(t)\cos(2\pi f_c t + \phi(t)), \quad (1)$$

where $A(t)$ and $\phi(t)$ are the time-varying amplitude and phase, respectively. After splitting the carrier frequency, a

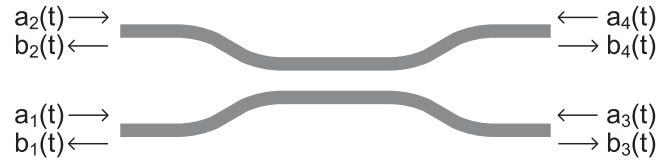


Fig. 1. Forward and backward waves at each port of a directional coupler.

corresponding baseband equivalent signal $a_l(t)$ can be derived

$$a_l(t) = A(t)e^{j\phi(t)}, \quad (2)$$

which is also the complex envelope of the signal $a(t)$. In order to obtain a corresponding baseband state-space model, the technique [7] starts by computing a pole-residue representation of the scattering parameters of the n -ports photonic system considered, in the form:

$$\mathbf{S}(s) = \sum_{k=1}^K \frac{\mathbf{R}_k}{s - p_k} + \mathbf{D}_{VF}, \quad (3)$$

where s is the Laplace variable, \mathbf{S} is the scattering matrix of the system under study, the poles p_k and residues $\mathbf{R}_k \in \mathbb{C}^{n \times n}$ are real or complex conjugate pairs, and the matrix $\mathbf{D}_{VF} \in \mathbb{R}^{n \times n}$ represents a constant term. In particular, the model (3) is computed by means of the VF algorithm, which allows one to guarantee the model stability by construction and to enforce its passivity through suitable passivity enforcement techniques [12]–[14]. Different possible approaches exist to convert a pole-residue model in the form (3) into a state-space representation, such as the Gilbert realization [15]. In particular, the method described in [7] converts the model (3) into a complex-valued state-space model, in the form:

$$\begin{cases} \frac{d\mathbf{x}(t)}{dt} = \mathbf{A}_{VF}\mathbf{x}(t) + \mathbf{B}_{VF}\mathbf{a}(t) \\ \mathbf{b}(t) = \mathbf{C}_{VF}\mathbf{x}(t) + \mathbf{D}_{VF}\mathbf{a}(t), \end{cases} \quad (4)$$

where $\mathbf{a}(t) \in \mathbb{R}^{n \times 1}$ and $\mathbf{b}(t) \in \mathbb{R}^{n \times 1}$ are the forward and backward waves, respectively, at the input and output ports of the system considered, as indicated in Fig. 1 for a directional coupler. The symbol $\mathbf{x}(t) \in \mathbb{R}^{m \times 1}$ is the state vector, while the state-space matrices are $\mathbf{A}_{VF} \in \mathbb{C}^{m \times m}$, $\mathbf{B}_{VF} \in \mathbb{R}^{m \times n}$, $\mathbf{C}_{VF} \in \mathbb{C}^{n \times m}$, $\mathbf{D}_{VF} \in \mathbb{R}^{n \times n}$, with $m = nK$. In particular, \mathbf{A}_{VF} is a diagonal matrix with all the poles as diagonal entries, while the elements in \mathbf{B}_{VF} are zeros and ones, and \mathbf{C}_{VF} contains all the residues [16].

Then, time-domain simulations can be carried out by solving the system of first-order ODE (4) via suitable numerical techniques. These approaches iteratively integrate (4) for a discrete set of values of the time, which are chosen via suitable algorithms (i.e. fixed or adaptive time-step). However, given that the time step to be adopted depends on the bandwidth of the signals considered, directly solving (4) with respect to signals at optical frequencies (e.g. 200 THz) in the form (1) can be computationally expensive, because it requires a prohibitively small time step [7].

Hence, the technique presented in [7] computes an equivalent baseband representation as

$$\begin{cases} \frac{d\mathbf{x}_l(t)}{dt} = (\mathbf{A}_{VF} - j2\pi f_c \mathbf{I}_m) \mathbf{x}_l(t) + \mathbf{B}_{VF} \mathbf{a}_l(t) \\ \mathbf{b}_l(t) = \mathbf{C}_{VF} \mathbf{x}_l(t) + \mathbf{D}_{VF} \mathbf{a}_l(t), \end{cases} \quad (5)$$

where $\mathbf{a}_l(t)$, $\mathbf{b}_l(t)$ and $\mathbf{x}_l(t)$ are the baseband equivalent signals in the form (2) of $\mathbf{a}(t)$, $\mathbf{b}(t)$ and $\mathbf{x}(t)$, respectively, while \mathbf{I}_m is the identity matrix of size $m \times m$. It is important to remark that, since \mathbf{A}_{VF} is a diagonal matrix with all the poles as diagonal entries, the operation $(\mathbf{A}_{VF} - j2\pi f_c \mathbf{I}_m)$ represents a shifting of all poles by the quantity $j2\pi f_c$ in the complex plane: the frequency response of the system described by the state-space matrices in (5) is shifted from the optical frequency range to baseband. Furthermore, it is proven that the baseband model (5) is stable and passive by construction, if the model (4) is stable and passive as well [7]. Finally, the system of ODE (5) can be efficiently simulated at baseband with relatively large time-steps with respect to (4), and the original port signals $\mathbf{a}(t)$, $\mathbf{b}(t)$ in (4) can be analytically computed starting from their corresponding baseband representation $\mathbf{a}_l(t)$, $\mathbf{b}_l(t)$ in (5).

III. NOVEL BASEBAND MODELING FRAMEWORK OF LINEAR PHOTONIC SYSTEMS

A general linear, passive, and time-invariant physical system can always be described by real-valued state-space models. They are widely used in the electronics and control theory fields where complex models, such as (4), are rarely used. Therefore, to make maximum use of such techniques for photonic circuit modeling, it is important to extend the baseband modeling technique in [7] to general real-valued state-space representations of linear photonic systems.

Let us assume that a general, linear and passive n -ports photonic system can be represented by a stable and passive state-space model operating at optical frequencies in the form:

$$\begin{cases} \frac{d\mathbf{x}(t)}{dt} = \mathbf{A}\mathbf{x}(t) + \mathbf{B}\mathbf{a}(t) \\ \mathbf{b}(t) = \mathbf{C}\mathbf{x}(t) + \mathbf{D}\mathbf{a}(t), \end{cases} \quad (6)$$

where $\mathbf{A} \in \mathbb{R}^{m \times m}$, $\mathbf{B} \in \mathbb{R}^{m \times n}$, $\mathbf{C} \in \mathbb{R}^{n \times m}$, $\mathbf{D} \in \mathbb{R}^{n \times n}$. It is important to note that \mathbf{A} , \mathbf{B} , \mathbf{C} , \mathbf{D} in (6) are assumed as matrices with real elements: such model can be obtained by means of the VF algorithm through a suitable conversion of the rational model (3) (see, for example, the method described in [16]), but also from other approaches, such as MOR techniques [17].

Now, starting from (6), it is possible to derive an equivalent complex-valued baseband state-space model by applying the same procedure described in [7] and summarized in Appendix A. In the following, we define such model as *general complex-valued baseband state-space model* in the form:

$$\begin{cases} \frac{d\mathbf{x}_l(t)}{dt} = (\mathbf{A} - j2\pi f_c \mathbf{I}_m) \mathbf{x}_l(t) + \mathbf{B} \mathbf{a}_l(t) \\ \mathbf{b}_l(t) = \mathbf{C} \mathbf{x}_l(t) + \mathbf{D} \mathbf{a}_l(t), \end{cases} \quad (7)$$

which demonstrates that the baseband modeling approach in [7] is not only applicable to a specific complex realization of the state-space matrices obtained via VF, but also to any general state-space model. It is important to note that the frequency response of the complex-valued model (7) is the frequency response of the model (6) shifted by the carrier frequency f_c . Indeed, expressing (7) into the Laplace domain leads to

$$\begin{aligned} \mathbf{S}_l(s) &= \mathbf{C} ((s + j2\pi f_c) \mathbf{I}_m - \mathbf{A})^{-1} \mathbf{B} + \mathbf{D} \\ &= \mathbf{S}(s + j2\pi f_c), \end{aligned} \quad (8)$$

where $\mathbf{S}_l(s)$ and $\mathbf{S}(s)$ are the transfer functions of the models (7) and (6) in the Laplace domain, respectively. Hence, the frequency response of the model (7) is not symmetrical with respect to positive and negative frequencies, which makes the baseband equivalent model a non-physical, complex-valued system.

The stability and passivity of the model (7), which are fundamental properties for time-domain simulations [11], are now investigated. In [7] a thorough discussion on the definition of the stability and passivity criteria for baseband systems is presented. Here it is sufficient to remark that the same methods to assess the stability and passivity of the state-space models of physical systems can be employed for baseband models as well [7]. In particular, the stability of a (complex- or real-valued) state-space model can be assessed by the eigenvalues of the matrix \mathbf{A} : the model is stable if the real part of all the eigenvalues is negative [18]. Now, let us assume that we start off with a realistic system (6) that is stable (e.g. any passive linear optical filter circuit), and the corresponding matrix \mathbf{A} is diagonalizable, where

$$\mathbf{A} = \mathbf{T}\mathbf{V}\mathbf{T}^{-1}, \quad (9)$$

and \mathbf{T} comprises all the eigenvectors and \mathbf{V} is a diagonal matrix whose elements are the corresponding eigenvalues. Note that all the eigenvalues in \mathbf{V} have negative real parts, since the state-space model (6) is assumed to be stable. Then, it is easy to derive

$$\mathbf{A} - j2\pi f_c \mathbf{I}_m = \mathbf{T}(\mathbf{V} - j2\pi f_c \mathbf{I}_m) \mathbf{T}^{-1}, \quad (10)$$

which indicates that the eigenvalues of the baseband model (7) are the ones of the model (6) shifted over $j2\pi f_c$ along the imaginary axis in the complex plane. Hence, the baseband model (7) is also stable (all the eigenvalues of the matrix $\mathbf{A} - j2\pi f_c \mathbf{I}_m$, have negative real parts) if the original state-space model (6) is stable.

The passivity of stable models can be verified by means of the corresponding Hamiltonian matrix [7], which for the system (7) is

$$\mathbf{M}_l = \begin{bmatrix} \mathbf{A}_l - \mathbf{B}\mathbf{L}^{-1}\mathbf{D}^H\mathbf{C} & -\mathbf{B}\mathbf{L}^{-1}\mathbf{B}^H \\ \mathbf{C}^H\mathbf{Q}^{-1}\mathbf{C} & -\mathbf{A}_l^H + \mathbf{C}^H\mathbf{D}\mathbf{L}^{-1}\mathbf{B}^H \end{bmatrix}, \quad (11)$$

where \mathbf{B} , \mathbf{C} , \mathbf{D} are the real state-space matrices in (7), while $\mathbf{A}_l = \mathbf{A} - j2\pi f_c \mathbf{I}_m$, $\mathbf{L} = \mathbf{D}^H\mathbf{D} - \mathbf{I}_n$ and $\mathbf{Q} = \mathbf{D}\mathbf{D}^H - \mathbf{I}_n$. Note that for real-valued systems the transpose operator T is used in the Hamiltonian matrix [16], but in a complex-valued system the transpose conjugate operator H is required [7]. In

particular, a (complex- or real-valued) stable state-space model is passive if its Hamiltonian matrix has no purely imaginary eigenvalues, since any purely imaginary eigenvalue indicates a crossover frequency where a singular value of the scattering matrix changes from being smaller to larger than unity, or vice versa [7], [16]. In the following, it is proven that the general complex-valued baseband state-space model (7) is passive by construction if the original model (6) is passive as well.

Indeed, the Hamiltonian matrix M for the real-valued model (6) can be represented by [16]

$$M = \begin{bmatrix} A - BL^{-1}D^T C & -BL^{-1}B^T \\ C^T Q^{-1}C & -A^T + C^T DL^{-1}B^T \end{bmatrix}. \quad (12)$$

By comparing (11) and (12), it is clear that

$$M_l = M - j2\pi f_c I_{2m}. \quad (13)$$

In [7] we have proven that, if (13) holds, it is possible to write:

$$\lambda_{li} = \lambda_i - j2\pi f_c, \quad (14)$$

where λ_{li} and λ_i with $i = 1, \dots, 2m$ are the eigenvalues of M_l and M , respectively. Hence, the baseband model (7) is passive (the Hamiltonian matrix M_l has no purely imaginary eigenvalues) if the original state-space model (6) is passive.

The methodology here presented extends the modeling power of the technique [7], while preserving its main advantages: robustness in the model-building phase and efficiency in time-domain simulations. In particular, the model stability and passivity can be guaranteed by enforcing the same properties on the model (6) computed at optical frequencies. If the VF algorithm is adopted, the model stability can be guaranteed by construction and its passivity can be enforced through robust passivity enforcement techniques [12]–[14].

IV. REAL-VALUED BASEBAND STATE-SPACE MODELS

Baseband state-space models represented by (5) and (7) are systems of first-order ODE and can be simulated only in solvers which support complex-valued signals and matrices. Whereas this complex system is compact and elegant, many solver techniques are developed and optimized for real-valued systems, such as SPICE, Verilog-A. In this section, a new real-valued baseband state-space model is derived starting from the modeling framework described in Section III, and its stability and passivity are investigated.

A. Model Derivation

Complex signals can be represented with respect to their real and imaginary parts, such as for $\mathbf{a}_l(t)$

$$\mathbf{a}_l(t) = \mathbf{a}_{lreal}(t) + j\mathbf{a}_{limag}(t). \quad (15)$$

By expressing all the complex signals in (7) in the form of (15) and by solving separately with respect to the real and the

imaginary parts, lead to:

$$\begin{cases} \frac{d\mathbf{x}_{lreal}(t)}{dt} = \mathbf{A}\mathbf{x}_{lreal}(t) + 2\pi f_c \mathbf{x}_{limag}(t) + \mathbf{B}\mathbf{a}_{lreal}(t) \\ \frac{d\mathbf{x}_{limag}(t)}{dt} = \mathbf{A}\mathbf{x}_{limag}(t) - 2\pi f_c \mathbf{x}_{lreal}(t) + \mathbf{B}\mathbf{a}_{limag}(t) \\ \mathbf{b}_{lreal}(t) = \mathbf{C}\mathbf{x}_{lreal}(t) + \mathbf{D}\mathbf{a}_{lreal}(t) \\ \mathbf{b}_{limag}(t) = \mathbf{C}\mathbf{x}_{limag}(t) + \mathbf{D}\mathbf{a}_{limag}(t). \end{cases} \quad (16)$$

It is important to remark that (16), which is a real system of ODE, can only be derived starting from the baseband state-space model (7) where \mathbf{A} , \mathbf{B} , \mathbf{C} , \mathbf{D} are real matrices: the model formulation originally proposed in [7] cannot be used to obtain (16). Then, by defining

$$\hat{\mathbf{a}}(t) = \begin{bmatrix} \mathbf{a}_{lreal}(t) \\ \mathbf{a}_{limag}(t) \end{bmatrix}, \quad \hat{\mathbf{b}}(t) = \begin{bmatrix} \mathbf{b}_{lreal}(t) \\ \mathbf{b}_{limag}(t) \end{bmatrix}, \quad \hat{\mathbf{x}}(t) = \begin{bmatrix} \mathbf{x}_{lreal}(t) \\ \mathbf{x}_{limag}(t) \end{bmatrix} \quad (17)$$

and

$$\begin{aligned} \hat{\mathbf{A}} &= \begin{bmatrix} \mathbf{A} & 2\pi f_c \mathbf{I}_m \\ -2\pi f_c \mathbf{I}_m & \mathbf{A} \end{bmatrix}, & \hat{\mathbf{B}} &= \begin{bmatrix} \mathbf{B} & \mathbf{0} \\ \mathbf{0} & \mathbf{B} \end{bmatrix}, \\ \hat{\mathbf{C}} &= \begin{bmatrix} \mathbf{C} & \mathbf{0} \\ \mathbf{0} & \mathbf{C} \end{bmatrix}, & \hat{\mathbf{D}} &= \begin{bmatrix} \mathbf{D} & \mathbf{0} \\ \mathbf{0} & \mathbf{D} \end{bmatrix}, \end{aligned} \quad (18)$$

where $\mathbf{0}$ represent the null matrix, equation (16) can be written as

$$\begin{cases} \frac{d\hat{\mathbf{x}}(t)}{dt} = \hat{\mathbf{A}}\hat{\mathbf{x}}(t) + \hat{\mathbf{B}}\hat{\mathbf{a}}(t) \\ \hat{\mathbf{b}}(t) = \hat{\mathbf{C}}\hat{\mathbf{x}}(t) + \hat{\mathbf{D}}\hat{\mathbf{a}}(t), \end{cases} \quad (19)$$

which is defined as *real-valued baseband state-space model*.

It is important to remark the key difference of the novel representation (19) with respect to the complex-valued baseband models (5) and (7). Indeed, the models (5) and (7) are pure mathematical representations of the system under study: their frequency response is not symmetrical with respect to positive and negative frequencies, and their impulse response is not real: even with real input signals, they can generate a complex output [7]. The novel macromodel (19) has a symmetrical frequency response with respect to positive and negative frequencies and its impulse response, input and output signals are real. Hence, it retains all properties of a physical system. It is defined as real-valued baseband state-space model since it can be simulated at the frequencies of the electronic modulating signal(s) rather than at optical frequencies, as for the complex-valued baseband models (5) and (7), thus achieving a significant speed-up in terms of efficiency with respect to models of photonic systems in the form (4) and (6). Furthermore, the novel model (19) is a system of first-order *real-valued* ODE, thereby it can be solved in a wider range of simulators than the complex models (5) and (7), which opens up the possibility of directly simulating passive photonic circuits with electronic ones. As remarked in the introduction, photonic-electronic co-simulations are of paramount importance [1]–[4], [19], [20]. This topic will be investigated in future contributions.

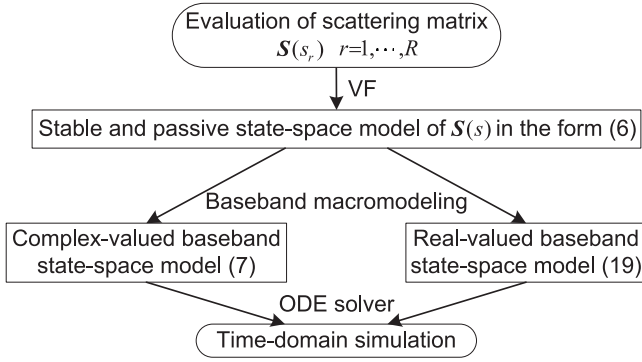


Fig. 2. Flowchart of the proposed baseband modeling framework for the time-domain simulation of photonic systems.

The novel model (19) still represents the same system as (7), but all the signals (originally complex) are now split into two real-valued signals representing their real and imaginary parts, which are coupled in the system of ODE (19). However, the size of (19) is doubled compared to (7) in terms of number of ports and state variables, since the signals of (19) are the real and imaginary parts of the signals in (7). This could have an impact in terms of simulation efficiency, but the model (19) maintains a high level of sparsity as well, as indicated in (18). It is important to remark that the novel real-valued baseband model (19) has been derived in this section starting from model (7). However, it can be directly computed starting from the state-space model (6), as indicated in equation (18). Hence, the calculation of the complex-valued baseband model (7) is not necessary to obtain the model (19). The flowchart in Fig. 2 shows the proposed baseband modeling framework in the case the VF algorithm is adopted to build the model (6).

B. Stability and Passivity Analysis

Since the model (19) can be considered as a real, linear, and time-invariant system with real input and output signals, the stability and passivity conditions defined for physical linear systems [18], such as (6), still hold for the new model (19).

The stability of a state-space model can be assessed by the eigenvalue of the matrix \hat{A} , as indicated in Section III: the model is stable if the real part of all the eigenvalues is negative [18]. Let us indicate the eigenvalues of \hat{A} with the symbol \hat{V}_k for $k = 1, \dots, 2m$ and the eigenvalues of A with V_k for $k = 1, \dots, m$. Starting from (18), it is proven in Appendix B that

$$\hat{V}_{2k-1,2k} = V_k \pm j2\pi f_c. \quad (20)$$

Hence, the real part of the eigenvalues of \hat{A} is the same as the eigenvalues of A : the model (19) is stable if the original model at optical frequencies is stable.

Then, as indicated in Section III, the passivity of the model (19) can be verified by means of its Hamiltonian matrix, which can be written as:

$$\hat{M} = \begin{bmatrix} \hat{M}_{11} & \hat{M}_{12} \\ \hat{M}_{21} & \hat{M}_{22} \end{bmatrix}, \quad (21)$$

where

$$\hat{M}_{11} = \begin{bmatrix} A - BL^{-1}D^T C & 2\pi f_c I_m \\ -2\pi f_c I_m & A - BL^{-1}D^T C \end{bmatrix},$$

$$\hat{M}_{12} = \begin{bmatrix} -BL^{-1}B^T & 0 \\ 0 & -BL^{-1}B^T \end{bmatrix},$$

$$\hat{M}_{21} = \begin{bmatrix} C^T Q^{-1} C & 0 \\ 0 & C^T Q^{-1} C \end{bmatrix},$$

$$\hat{M}_{22} = \begin{bmatrix} -A^T + C^T DL^{-1}B^T & 2\pi f_c I_m \\ -2\pi f_c I_m & -A^T + C^T DL^{-1}B^T \end{bmatrix}.$$

It is not surprising that the Hamiltonian matrix for (19) can be expressed in terms of block matrices, given that the state-space matrices for the real-valued baseband state-space model are block matrices as well, as indicated in (18).

By performing a similarity transformation, the matrix \bar{M} can be obtained

$$\bar{M} = P \hat{M} P^{-1} = \begin{bmatrix} M & 2\pi f_c I_{2m} \\ -2\pi f_c I_{2m} & M \end{bmatrix}, \quad (22)$$

where

$$P = \begin{bmatrix} I_m & 0 & 0 & 0 \\ 0 & 0 & I_m & 0 \\ 0 & I_m & 0 & 0 \\ 0 & 0 & 0 & I_m \end{bmatrix}, \quad (23)$$

and M is the Hamiltonian matrix of the system (6), described in (12). Note that, the similarity transformation (22) is equivalent to row and column blocks exchanges and it can be derived by simple algebraic manipulations.

Since similarity transformations of matrices do not change their eigenvalues, \bar{M} and \hat{M} share the same set of eigenvalues Λ_k with $k = 1, \dots, 4m$. Now, by following the procedure described in Appendix B, it is proven that

$$\Lambda_{2i-1,2i} = \lambda_i \pm j2\pi f_c, \quad (24)$$

where λ_i with $i = 1, \dots, 2m$ are the eigenvalues of M . Equation (24) proves that the eigenvalues of \bar{M} and \hat{M} share the same real parts with the ones of M : the model (19) is passive (\hat{M} has no purely imaginary eigenvalue) if the model (6) is passive.

Hence, this section demonstrates that the stability and passivity of the new model (19) are directly determined by the properties of the original model (6), and the following statements hold:

- One unstable eigenvalue (whose real part is positive) of (6) leads to two unstable eigenvalues of the model (19).
- One crossover frequency point where a passivity violation occurs for (6) leads to two crossover frequency points for the model (19).

V. EXAMPLES ON PHOTONIC CIRCUITS

This section presents two application examples of the proposed modeling and simulation techniques. The scattering

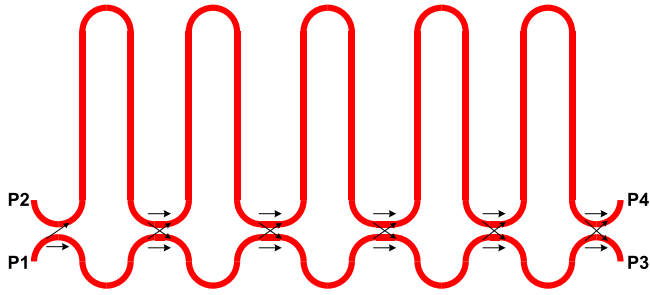


Fig. 3. The geometric structure of the Mach-Zehnder interferometer lattice filter.

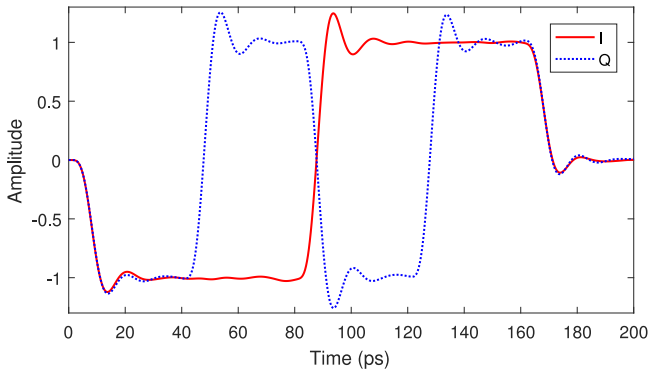


Fig. 4. The modulating signals: in-phase part $I(t)$ and quadrature part $Q(t)$.

parameters of the photonic systems under study are evaluated via the *Caphe* circuit simulator (Luceda Photonics) and electromagnetic simulations in *FDTD Solutions* (Lumerical), while the time-domain simulations are carried out in Matlab on a personal computer with Intel Core i3 processor and 8 GB RAM. It is important to remark that, even though *Caphe* and *FDTD Solutions* are chosen to estimate the scattering parameters in the proposed examples, there is no limitation on adopting any other simulator.

A. Lattice Filter

A fifth order finite impulse response filter with a Chebyshev window is realized via a Mach-Zehnder interferometer lattice filter, shown in Fig. 3. The filter characteristics are described in [7].

Let us assume that port $P1$ of the filter is excited by a 4-QAM (*quadrature phase-shift keying*) modulated optical signal with carrier frequency $f_c = 195.11$ THz and the in-phase $I(t)$ and quadrature component $Q(t)$ are four bits sequences $(-1, -1, 1, 1)$ and $(-1, 1, -1, 1)$, respectively, as shown in Fig. 4 where overshoot and undershoot are present to mimic realistic radio frequency (RF) signals. Note that $I(t)$ and $Q(t)$ are the real and imaginary parts of the baseband equivalent signals (2), respectively [7]. It is important to remark that any RF signal with generic shape can be adopted here, as long as the chosen modeling frequencies cover the spectrum of the signal [7].

The scattering parameters of the filter are simulated in *Caphe* in the frequency range $[f_c - \Delta; f_c + \Delta]$, where $\Delta = 380$ GHz, in order to guarantee that the chosen range covers the spectrum

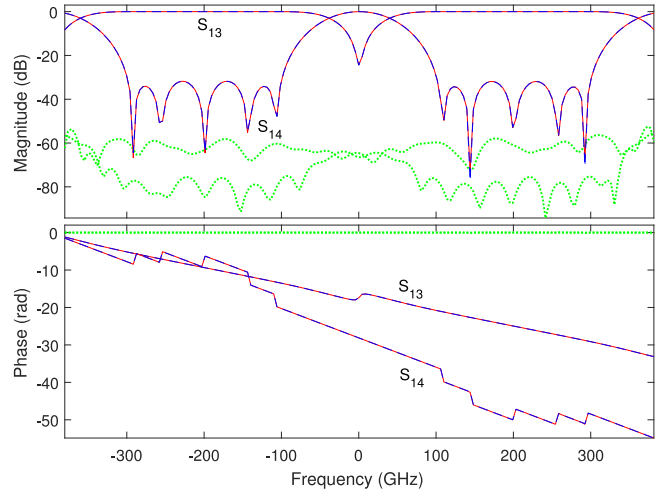


Fig. 5. Magnitude (top) and phase (bottom) of the lattice filter baseband scattering parameters extracted via *Caphe* (full blue line) and computed via the complex-valued baseband state-space model (7) (red dashed line), where the green dots represent the corresponding absolute error.

of the modulated optical signal. In this example, 181 frequency samples are used and they are uniformly distributed over the frequency range of interest. Adaptive sampling strategies can also be adopted to choose the frequency samples efficiently: more samples are chosen where the frequency response is dynamic, such as resonances, and less are chosen in smooth areas [18]. Next, a state-space model is built with 39 poles via the VF algorithm, achieving a maximum absolute error of less than -50 dB. A standard bottom-up approach is used to select the required number of poles [18], [21]: the initial number of poles is iteratively increased until the desired accuracy of -50 dB is reached. In particular, the state-space model computed is formed only by real-valued matrices, as in (6). Note that, the time-domain simulation of this model computed at optical frequencies will be used in the following as a reference to validate the accuracy and the efficiency of the proposed method.

Next, the corresponding complex-valued baseband state-space model in the form (7) can be easily computed. The frequency-domain accuracy of such model is illustrated in Fig. 5, where a comparison between the model frequency response and the corresponding baseband scattering parameters (obtained by translating the scattering parameters simulated in *Caphe* into baseband) is shown. Finally, a real-valued baseband state-space model in the form (19) has been computed by following the procedure described in Section IV.

The simulations of the three models (namely, (6), (7), and (19)) are carried out with the Matlab routine *lsim*, and require 10 s, 0.12 s and 0.11 s, respectively. The main speed-up factor of the proposed modeling approach is given by the adopted time-step: the model (6) requires a time step of 0.25 fs, while the baseband models (7) and (19) are simulated with a time step of 0.33 ps.

It is important to remark that the output of model (7) is a complex signal and its magnitude corresponds to the envelope of the output of model (6), as illustrated in Fig. 6. Furthermore, it is always possible to analytically reconstruct the port signals of

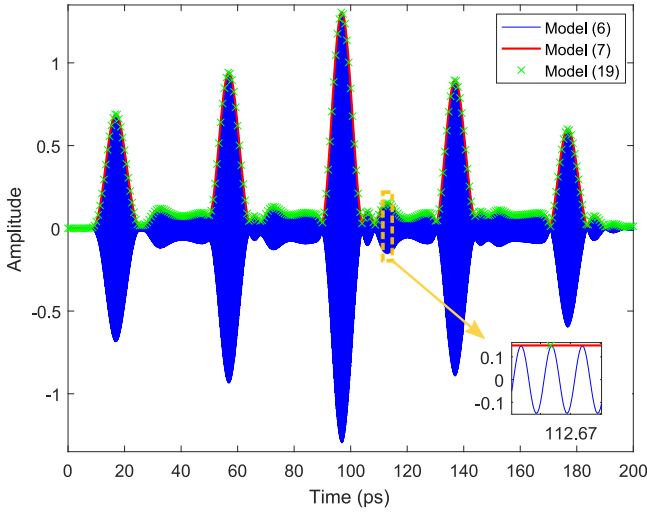


Fig. 6. Output signal at port $P3$ of the lattice filter. The blue line represents the signal obtained from model (6), while the red line and green cross represent the absolute value of the complex signal obtained by the time-domain simulation of (7) and (19).

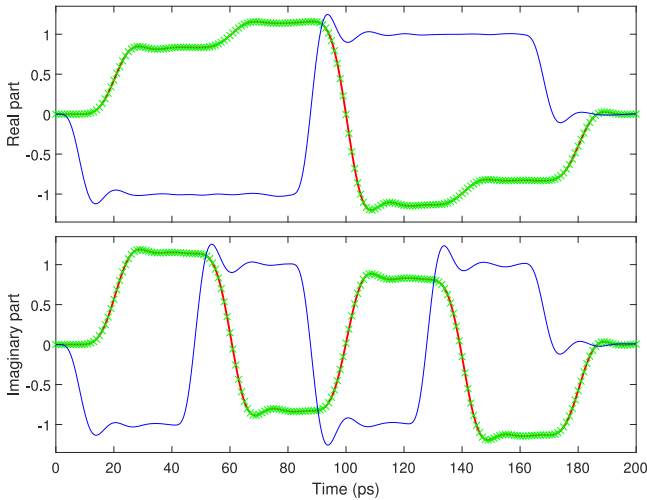


Fig. 7. Real (top) and imaginary (bottom) parts of the output signal at port $P4$ of the lattice filter obtained via the models (7) and (19), where the solid red lines and green crosses represent the results from (7) and (19), respectively, while the blue solid lines are the corresponding real and imaginary parts of the input signal at port $P1$.

the photonic system under study starting from the time-domain simulation of the corresponding baseband equivalent model [7]. Finally, Fig. 6 shows the baseband complex signals computed from the outputs of model (19), according to (15) and (16). It is evident that the time-domain simulation results of the two novel proposed models (7) and (19) are in excellent agreement with the reference solution obtained via the model (6). As additional proof of the accuracy of the proposed modeling strategies, a comparison of the real and imaginary part of the complex baseband signal at port $P4$ obtained by the complex- and real-valued baseband models is shown in Fig. 7: the results demonstrate a very good match.

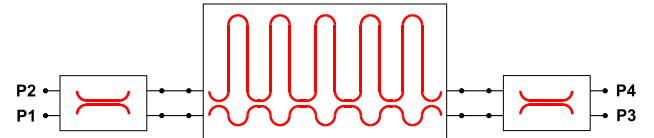


Fig. 8. The schematic structure of the photonic circuit under study.

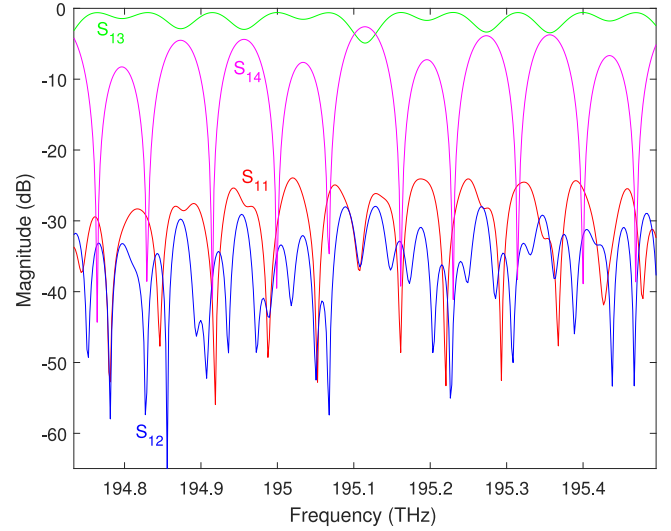


Fig. 9. Frequency response of the photonic circuit in Fig. 8 in the frequency range of interest.

B. Circuit Simulation

The simulation of the photonic circuit shown in Fig. 8, formed by two directional couplers and a lattice filter, is described in the following. The lattice filter is the one presented in the previous section, while the two identical directional couplers have $20 \mu\text{m}$ coupling length, $5 \mu\text{m}$ bend radius, and $0.15 \mu\text{m}$ gap between coupling waveguides, whose width is $0.43 \mu\text{m}$.

In order to simulate this circuit, the baseband models for each device in Fig. 8 are computed first, and then properly connected. Since the 4-QAM modulating signal (with same carrier frequency) described in Section V-A is used to excite the circuit at port $P1$, the scattering parameters of the directional coupler are evaluated in the Lumerical FDTD solver for the same frequency range used for the lattice filter, namely $[f_c - \Delta; f_c + \Delta]$, where $\Delta = 380 \text{ GHz}$. Considering that the frequency response is rather smooth over the frequency range of interest, only 30 equidistantly spread frequency samples are selected for building the model. It is important to note that the scattering parameters of the lattice filter are evaluated in Caphe and its Caphe model is an ideal model without considering reflections, while the directional coupler is simulated in Lumerical FDTD solver where the reflection at each port is modeled. Fig. 9 shows the transmissions and reflections characteristics of the whole circuit under study. Then, a state-space model in the form (6) is built for the directional coupler via the VF algorithm with 14 poles, achieving an absolute maximum error of less than -50 dB . Finally, the corresponding complex- and real-valued baseband models

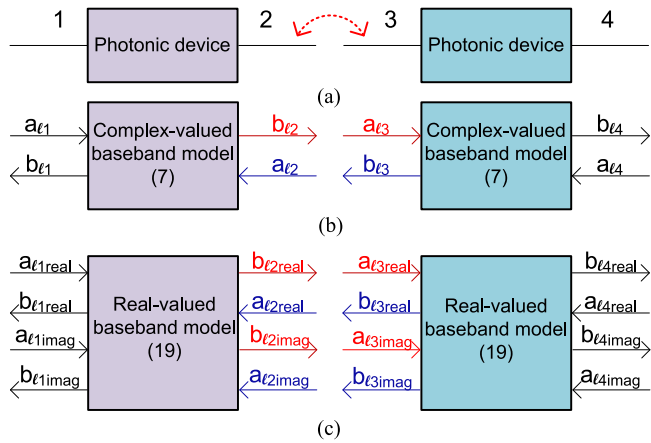


Fig. 10. Example of the connection of the baseband models of two-ports photonic devices. (a) The physical connection. (b) The connection of the corresponding complex-valued baseband state-space models (7). (c) The connection of the corresponding real-valued baseband state-space models (19).

are computed via the approaches outlined in Sections III and IV, respectively.

Once the models of the lattice filter and directional coupler have been obtained, they can be easily connected in order to describe the input/output behavior of the circuit under study. Fig. 10 shows an example of the connection of baseband models computed for two-ports devices. It is very intuitive to realize that the forward wave at port 3 in Fig. 10 is the backward one for port 2, and vice versa: the corresponding ports of the baseband models must be connected accordingly. The same principle applies to general types of connections (i.e. parallel, feedback, etc.) and for any number of ports. Now, the built complex-valued and real-valued baseband models can be readily connected via the *connect* routine in Matlab, following the method illustrated in Fig. 10, and the time-domain simulation can be performed via the dedicated linear system solver *lsim*. Note that any hierarchical connection can be realized via the *connect* routine, even though only the cascaded case is shown in this example.

Fig. 11 shows the magnitude of the complex baseband reflected signal at port $P1$ and transmission signal at port $P3$ obtained with the models (7) and (19), which again demonstrates the accuracy of the proposed techniques. The simulation of the complex- and real-valued models requires the same time: 0.42 s.

Rather than modeling each device separately, it is also possible to consider the entire circuit in Fig. 8 as a single passive element, described by its scattering parameters. Then, a state-space model in the form (6) can be built for the entire circuit with 69 poles via the VF algorithm, achieving a maximum absolute error of less than -50 dB. The corresponding complex- and real-valued baseband models can be calculated as described in Sections III and IV, respectively. Fig. 12 shows an example of the results of the two modeling strategies considered, namely *devices* and *circuit modeling*: the two approaches are in excellent agreement. This is a remarkable improvement compared with the FIR modeling technique, where the modeling

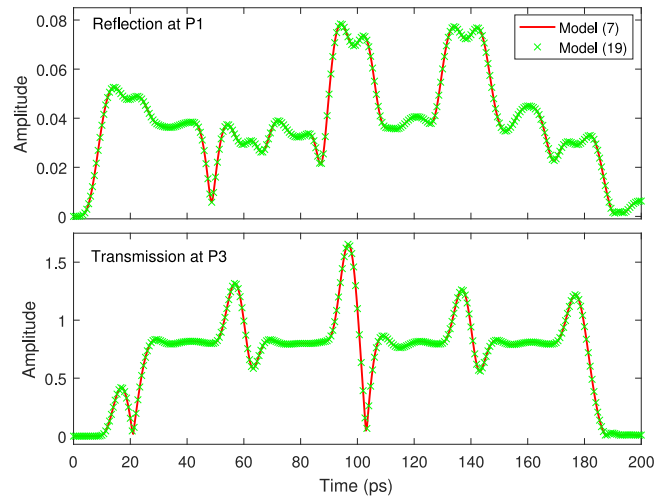


Fig. 11. The amplitude of the reflected signal at port $P1$ (top) and transmission signal at port $P3$ (bottom) of the circuit obtained from the simulations of the models (7) and (19) with excitation signal shown in Fig. 4.

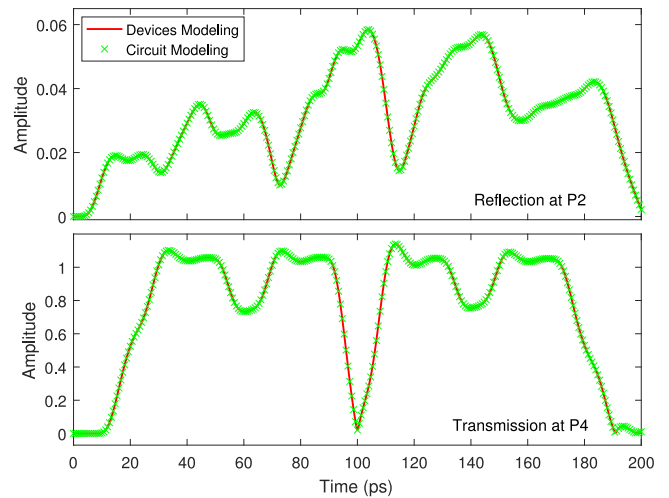


Fig. 12. The amplitude of the reflected signal at port $P2$ (top) and transmission signal at port $P4$ (bottom) of the circuit obtained by the real baseband model (19) computed via the devices and circuit modeling strategies.

accuracy could decrease significantly when multiples FIR models are connected [5].

The time-domain simulation of the baseband model obtained via the circuit modeling approach requires 0.43 s, a similar computational cost to the devices modeling approach, once again demonstrating the efficiency of the proposed method.

VI. CONCLUSION

This paper presented a technique to efficiently simulate photonic linear circuits with a complex-valued baseband representation by means of existing solvers that support only real-valued systems. It significantly extends the baseband modeling and simulation framework proposed in [7]. The complex-valued baseband model can be derived from general state-space models of linear photonic systems, and accurately simulated at

baseband with relative large time steps. For simulators which can only deal with real-valued models of physical systems, the complex-valued baseband models can now be analytically converted to real-valued ones immediately. Both kinds of baseband models can be proven stable and passive by construction if the original state-space models operating at optical frequency range are stable and passive. Two examples were presented to verify the accuracy and efficiency of the proposed technique.

APPENDIX A DERIVATION OF THE GENERAL COMPLEX-VALUED BASEBAND STATE-SPACE MODEL

The relation between the modulated signal $a(t)$ in (1) and its baseband equivalent $a_l(t)$ in (2) is given by [7]

$$a(t) = \text{Re}(a_l(t)e^{j2\pi f_c t}), \quad (25)$$

$$\mathcal{H}(a(t)) = \text{Im}(a_l(t)e^{j2\pi f_c t}), \quad (26)$$

where $\text{Re}(\cdot)$ and $\text{Im}(\cdot)$ stand for the real and imaginary parts, respectively, and $\mathcal{H}(\cdot)$ represents the Hilbert transform.

Now, expressing the signals and state vector of (6) in the form (25) gives

$$\begin{cases} \text{Re} \frac{d(\mathbf{x}_l(t)e^{j2\pi f_c t})}{dt} = \\ \quad \mathbf{A} \text{Re}(\mathbf{x}_l(t)e^{j2\pi f_c t}) + \mathbf{B} \text{Re}(\mathbf{a}_l(t)e^{j2\pi f_c t}) \\ \text{Re}(\mathbf{b}_l(t)e^{j2\pi f_c t}) = \\ \quad \mathbf{C} \text{Re}(\mathbf{x}_l(t)e^{j2\pi f_c t}) + \mathbf{D} \text{Re}(\mathbf{a}_l(t)e^{j2\pi f_c t}). \end{cases} \quad (27)$$

Next, by applying the Hilbert transform to (6) and using the relation (26) leads to

$$\begin{cases} \text{Im} \frac{d(\mathbf{x}_l(t)e^{j2\pi f_c t})}{dt} = \\ \quad \mathbf{A} \text{Im}(\mathbf{x}_l(t)e^{j2\pi f_c t}) + \mathbf{B} \text{Im}(\mathbf{a}_l(t)e^{j2\pi f_c t}) \\ \text{Im}(\mathbf{b}_l(t)e^{j2\pi f_c t}) = \\ \quad \mathbf{C} \text{Im}(\mathbf{x}_l(t)e^{j2\pi f_c t}) + \mathbf{D} \text{Im}(\mathbf{a}_l(t)e^{j2\pi f_c t}). \end{cases} \quad (28)$$

Combining (27) and (28) allows one to write

$$\begin{cases} \frac{d(\mathbf{x}_l(t)e^{j2\pi f_c t})}{dt} = \mathbf{A}\mathbf{x}_l(t)e^{j2\pi f_c t} + \mathbf{B}\mathbf{a}_l(t)e^{j2\pi f_c t} \\ \mathbf{b}_l(t)e^{j2\pi f_c t} = \mathbf{C}\mathbf{x}_l(t)e^{j2\pi f_c t} + \mathbf{D}\mathbf{a}_l(t)e^{j2\pi f_c t}. \end{cases} \quad (29)$$

After simple mathematical manipulations, (29) can be simplified to

$$\begin{cases} \frac{d\mathbf{x}_l(t)}{dt} = (\mathbf{A} - j2\pi f_c \mathbf{I}_m)\mathbf{x}_l(t) + \mathbf{B}\mathbf{a}_l(t) \\ \mathbf{b}_l(t) = \mathbf{C}\mathbf{x}_l(t) + \mathbf{D}\mathbf{a}_l(t), \end{cases} \quad (30)$$

which is the complex-valued baseband state-space model in (7).

APPENDIX B EIGENVALUES CALCULATION

Indicating one of the eigenvalues of $\hat{\mathbf{A}}$ with \hat{V}_k and considering (18), the following holds:

$$\left| \hat{\mathbf{A}} - \hat{V}_k \mathbf{I}_{2m} \right| = \left| \begin{bmatrix} \mathbf{A} - \hat{V}_k \mathbf{I}_m & 2\pi f_c \mathbf{I}_m \\ -2\pi f_c \mathbf{I}_m & \mathbf{A} - \hat{V}_k \mathbf{I}_m \end{bmatrix} \right| = 0, \quad (31)$$

where $|\cdot|$ stands for the determinant of a matrix. Thanks to (9), equation (31) can be written as

$$\left| \begin{bmatrix} \mathbf{T}(\mathbf{V} - \hat{V}_k \mathbf{I}_m) \mathbf{T}^{-1} & 2\pi f_c \mathbf{I}_m \\ -2\pi f_c \mathbf{I}_m & \mathbf{T}(\mathbf{V} - \hat{V}_k \mathbf{I}_m) \mathbf{T}^{-1} \end{bmatrix} \right| = 0. \quad (32)$$

Since the determinant operator in (32) is applied to a block matrix, it is possible to write equation (32) as [22]

$$\left| \mathbf{T}(\mathbf{V} - \hat{V}_k \mathbf{I}_m)^2 \mathbf{T}^{-1} + (2\pi f_c)^2 \mathbf{I}_m \right| = 0, \quad (33)$$

leading to

$$\left| \mathbf{T} \left((\mathbf{V} - \hat{V}_k \mathbf{I}_m)^2 + (2\pi f_c)^2 \mathbf{I}_m \right) \mathbf{T}^{-1} \right| = 0. \quad (34)$$

Hence, there must be a diagonal element V_i in \mathbf{V} satisfying

$$V_i^2 - 2V_i \hat{V}_k + \hat{V}_k^2 + (2\pi f_c)^2 = 0. \quad (35)$$

Solving (35) for \hat{V}_k gives

$$\hat{V}_k = \begin{cases} V_i + j2\pi f_c \\ V_i - j2\pi f_c \end{cases}, \quad (36)$$

which indicates that the eigenvalues of $\hat{\mathbf{A}}$ can be obtained by shifting the eigenvalues of \mathbf{A} along the imaginary axis in the complex plane by $\pm j2\pi f_c$.

REFERENCES

- [1] W. Bogaerts and L. Chrostowski, "Silicon photonics circuit design: Methods, tools and challenges," *Laser Photon Rev.*, vol. 12, no. 4, 2018, Art. no. 1700237.
- [2] Z. Zhang *et al.*, "Compact modeling for silicon photonic heterogeneously integrated circuits," *J. Lightw. Technol.*, vol. 35, no. 14, pp. 2973–2980, Jul. 2017.
- [3] C. Sorace-Agaskar, J. Leu, M. R. Watts, and V. Stojanovic, "Electro-optical co-simulation for integrated CMOS photonic circuits with VerilogA," *Opt. Express*, vol. 23, no. 21, pp. 27180–27203, Oct. 2015.
- [4] P. Gunupudi, T. Smy, J. Klein, and Z. J. Jakubczyk, "Self-consistent simulation of opto-electronic circuits using a modified nodal analysis formulation," *IEEE Trans. Adv. Packag.*, vol. 33, no. 4, pp. 979–993, Nov. 2010.
- [5] S. Mingaleev, A. Richter, E. Sokolov, C. Arellano, and I. Koltchanov, "Towards an automated design framework for large-scale photonic integrated circuits," *Proc. SPIE*, vol. 9516, 2015, Art. no. 951602.
- [6] J. Pond *et al.*, "A complete design flow for silicon photonics," *Proc. SPIE*, vol. 9133, 2014, Art. no. 913310.
- [7] Y. Ye, D. Spina, Y. Xing, W. Bogaerts, and T. Dhaene, "Numerical modeling of linear photonic system for accurate and efficient time-domain simulations," *Photon. Res.*, vol. 6, no. 6, pp. 560–573, Jun. 2018.
- [8] B. Gustavsen and A. Semlyen, "Rational approximation of frequency domain responses by vector fitting," *IEEE Trans. Power Del.*, vol. 14, no. 3, pp. 1052–1061, Jul. 1999.
- [9] D. Deschrijver and T. Dhaene, "Broadband macromodelling of passive components using orthonormal vector fitting," *Electron. Lett.*, vol. 41, no. 21, pp. 1160–1161, Oct. 2005.

- [10] D. Deschrijver, M. Mrozowski, T. Dhaene, and D. De Zutter, "Macromodeling of multiport systems using a fast implementation of the vector fitting method," *IEEE Microw. Compon. Lett.*, vol. 18, no. 6, pp. 383–385, Jun. 2008.
- [11] S. Grivet-Talocia and B. Gustavsen, "Black-box macromodeling and its EMC applications," *IEEE Electromagn. Compat. Mag.*, vol. 5, no. 3, pp. 71–78, Third Quarter 2016.
- [12] D. Saraswat, R. Achar, and M. S. Nakhla, "A fast algorithm and practical considerations for passive macromodeling of measured/simulated data," *IEEE Trans. Adv. Packag.*, vol. 27, no. 1, pp. 57–70, Feb. 2004.
- [13] B. Gustavsen, "Fast passivity enforcement for S-parameter models by perturbation of residue matrix eigenvalues," *IEEE Trans. Adv. Packag.*, vol. 33, no. 1, pp. 257–265, Feb. 2010.
- [14] D. Deschrijver and T. Dhaene, "Fast passivity enforcement of S-parameter macromodels by pole perturbation," *IEEE Trans. Microw. Theory Techn.*, vol. 57, no. 3, pp. 620–626, Mar. 2009.
- [15] E. Gilbert, "Controllability and observability in multivariable control systems," *SIAM J. Control*, vol. 1, no. 2, pp. 128–151, 1963.
- [16] B. Gustavsen and A. Semlyen, "Fast passivity assessment for S-parameter rational models via a half-size test matrix," *IEEE Trans. Microw. Theory Techn.*, vol. 56, no. 12, pp. 2701–2708, Dec. 2008.
- [17] R. Achar and M. S. Nakhla, "Simulation of high-speed interconnects," *Proc. IEEE*, vol. 89, no. 5, pp. 693–728, May 2001.
- [18] S. Grivet-Talocia and B. Gustavsen, *Passive Macromodeling: Theory and Applications*. Hoboken, NJ, USA: Wiley, 2015.
- [19] S. Tanaka, T. Usuki, and Y. Tanaka, "Accurate SPICE model of forward-biased silicon PIN Mach-Zehnder modulator for an energy-efficient multilevel transmitter," *J. Lightw. Technol.*, vol. 36, no. 10, pp. 1959–1969, May 2018.
- [20] B. Wang *et al.*, "A compact Verilog-A model of silicon carrier-injection ring modulators for optical interconnect transceiver circuit design," *J. Lightw. Technol.*, vol. 34, no. 12, pp. 2996–3005, Jun. 2016.
- [21] N. Stevens, D. Deschrijver, and T. Dhaene, "Fast automatic order estimation of rational macromodels for signal integrity analysis," in *Proc. IEEE Workshop Signal Propag. Interconnects*, Genova, Italy, May 2007, pp. 89–92.
- [22] P. D. Powell, "Calculating determinants of block matrices," 2011. [Online]. Available: <https://arxiv.org/abs/1112.4379>

Authors' biographies not available at the time of publication.